Electronic Supplementary Material (ESI) for Nanoscale.

Supporting Information

High-Performance Supercabatteries Using Graphite@Diamond Nano-needle Capacitor Electrodes and Redox Electrolytes

Siyu Yu,[a,b,§] Kamatchi Jothiramalingam Sankaran,[c,d,§] Svetlana Korneychuk,[e] Johan Verbeeck,[e] Ken Haenen,*[c,d] Xin Jiang,*[a] and Nianjun Yang*[a]

[§]equally contributed

[a]Institute of Materials Engineering, University of Siegen, Siegen 57076, Germany

[b]School of Chemistry and Chemical Engineering, Southwest University, Chongqing 400715, China

[c]Institute for Materials Research (IMO), Hasselt University, 3590 Diepenbeek, Belgium

[d]IMOMEC, IMEC vzw, 3590 Diepenbeek, Belgium

[e]Electron Microscopy for Materials Science (EMAT), University of Antwerp, 2020 Antwerp, Belgium

E-mail addresses: ken.haenen@uhasselt.be; xin.jiang@uni-siegen.de; nianjun.yang@uni-siegen.de

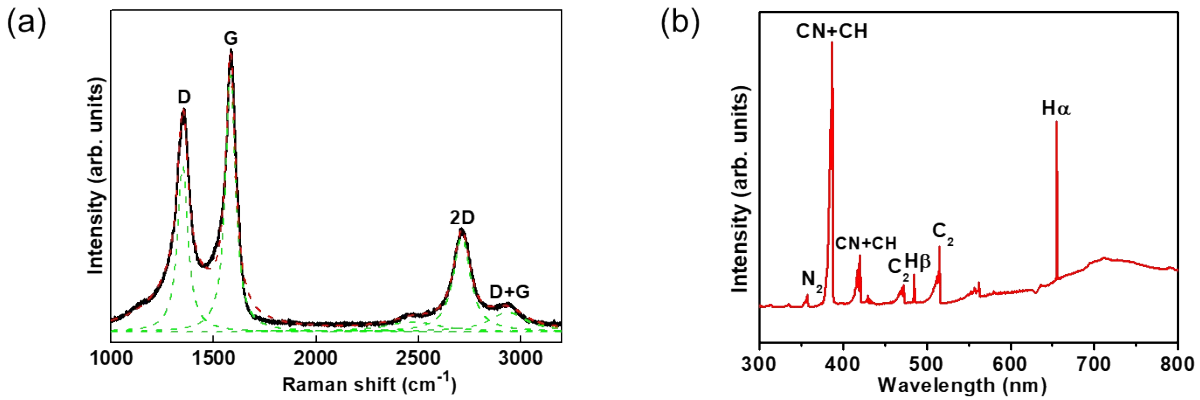

Figure S1. (a) Micro-Raman spectra of graphite@diamond nano-needles on a nitrogen-doped nanocrystalline diamond (N-NCD) film. The solid and dashed lines are experimental and simulated results, respectively. (b) The optical emission spectroscopy (OES) spectrum recorded during the growth of graphite@diamond nanoneedles using $CH_4/H_2/N_2$ plasmas.

The graphite@diamond nanoneedles were grown in a gas mixture of CH_4 (45 sccm) + H_2 (246 sccm) + N_2 (9 sccm) ($CH_4/H_2/N_2$=15/82/3), a microwave power of 3000 W, the total pressure of 65 Torr in the chamber, and the substrate temperature of around 780°C. To make the growth mechanism of graphite@diamond nanoneedles, the plasma constituents were recorded using *in situ* optical emission spectroscopy (OES, AvaSpec-2048 (Avantes)) measurements (**Figure S1b)**. The major peaks observed are: H_α at 655.3 and H_β at 486.0 nm representing the Balmer atomic hydrogen emission lines, the C_2 swan system at 516.0 nm, N_2 peak at 357.3 nm and the CN violet system at 387.3 nm and 418.1 nm, respectively.[S1-S3] N_2 and CN peaks were observed because of the incorporation of nitrogen. CH species are also present because of the dissociation of CH_4 species, however the CH band was totally overlapped by the CN band[S4] and hence, we named the peaks at 387.3 nm and 418.1 nm as CN+CH. Theoretically, it is revealed that the definite faces (for example (100) faces) of the nanodiamond clusters are preferentially attached by the CN species and encourage the formation of diamond nanoneedles.[S5] The CN species are adhered on the surface of the C_2 dimers that result in an anisotropic diamond growth in [100] direction, in which the energetically favorable CN molecule stays on the growth surface.[S5–S7] Moreover, previous studies[S8–S10] observed that above 700°C, the equi-axed like granular structure changes to needle-like structure because of the occurrence of large quantity of CN species. Together with the above-defined results, it is proven that the CN species are significant for the origin of nanoneedles for the

graphite@diamond nanoneedles. However, a high substrate temperature is necessary for triggering the CN species in inducing the attachment of C_2 species through the CN adhered surface. For the growth of graphite@diamond nanoneedles, the substrate temperature is 780 °C and hence CN species are dominant than CH species that leading to preferential attachment of C_2 species and inducing the anisotropic growth of diamond grains. Therefore, inside graphite@diamond nanoneedles the smaller grains start to combine along any desired direction, ensuing in high aspect ratio diamond nanoneedles. Moreover, during the anisotropic growth, the surface C atoms surrounding the sp^3-bonded diamond core tend to form sp^2-bonded carbon as it is energetic favorable. That is, it is a natural tendency on the formation of graphitic layers surrounding the anisotropic growth of diamond grains.

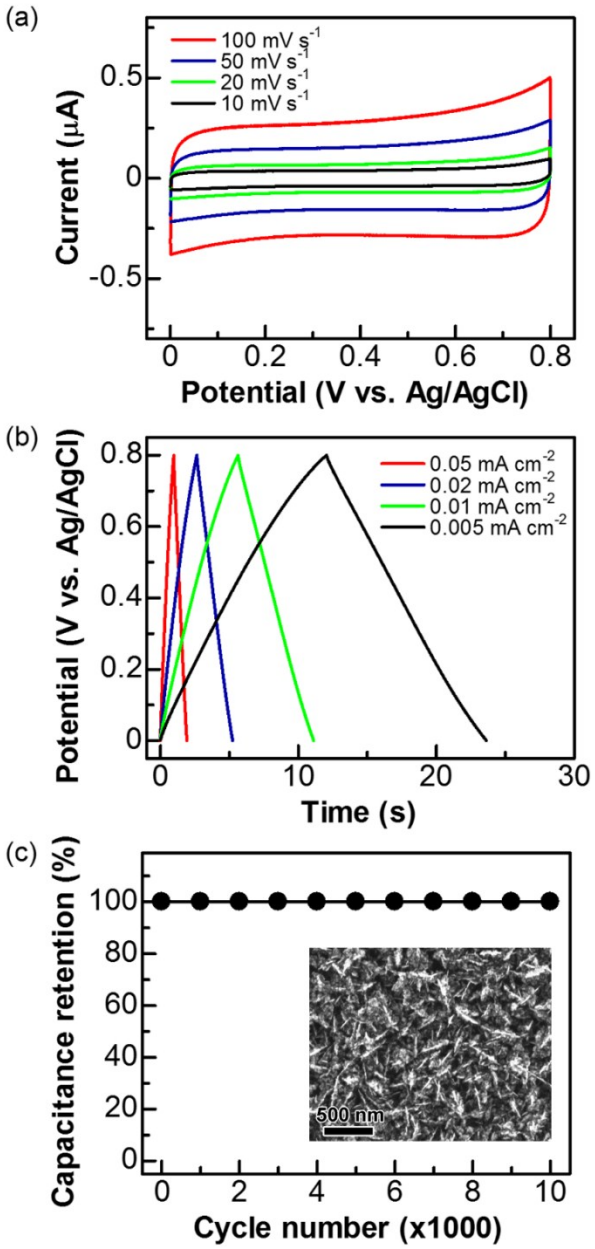

Figure S2. Capacitance performance of graphite@diamond nano-needles in an organic solution of 0.1 M tetrabutylammonium tetrafluoroborate ($TBABF_4$) in propylene carbonate: (a) cyclic voltammograms obtained at different scan rates; (b) galvanostatic charge/discharge curves at different current densities; (c) capacitance retention at a charge/discharge current of 0.02 mA cm^{-2}. The inset shows the SEM image of used N-NCD film after 10 000 charge/discharge cycles.

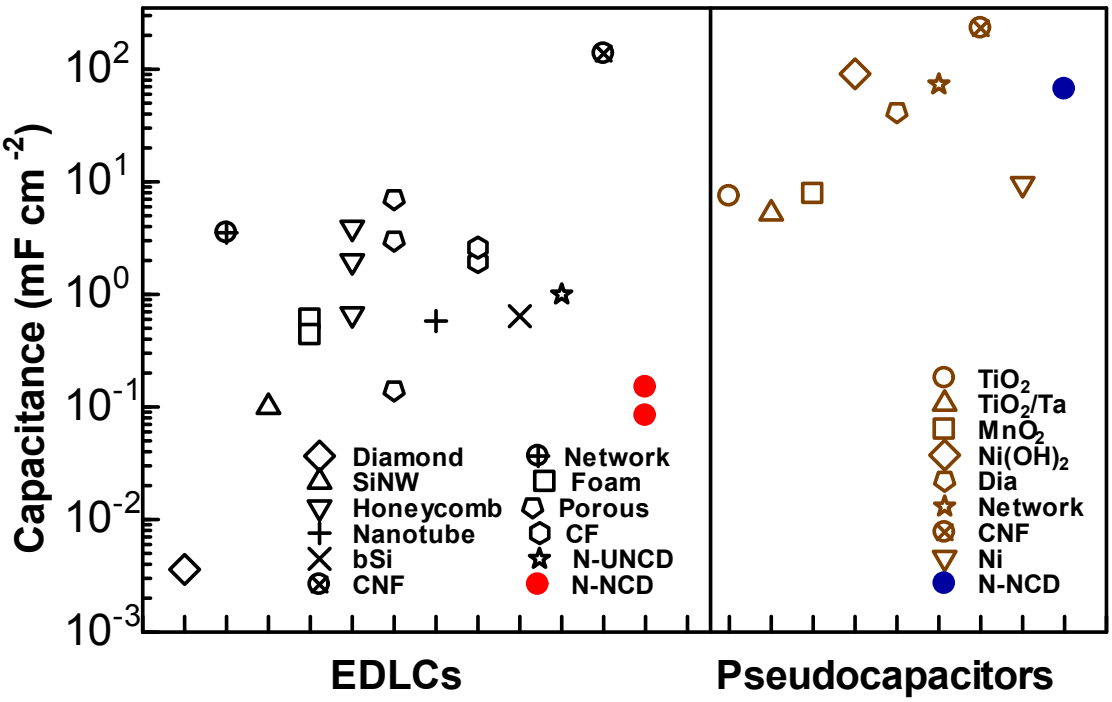

Figure S3. Capacitance comparison of diamond supercapacitors, including electrical double layer capacitors (EDLCs) and pseudocapacitors (PCs). The employed capacitor electrodes are: boron-doped diamond (BDD) network (Network)[S11], BDD/silicon nanowires (SiNW) [S12, S13], BDD foam (Foam) [S14], honeycomb BDD (Honeycomb) [S15- S17], porous BDD (Porous) [S18- S20], BDD/Nanotube (Nanotube) [S21], BDD/carbon fiber (CF) [S22, S23], BDD/'black silicon' (bSi) [S24], nitrogen-included ultra-nanocrystalline diamond (N-UNCD) [S25], carbon nanofiber/BDD (CNF) [S26], N-NCD (N-NCD, this work), BDD/TiO_2 (TiO_2) [S27-S29], TiO_2/BDD/Ta (TiO_2/Ta) [S30], MnO_2/BDD (MnO_2) [S31], $Ni(OH)_2$/diamond nanowire ($Ni(OH)_2$) [S32], Ni/porous BDD [S33]. For some PCs, redox electrolytes were introduced when different diamond electrodes were applied: BDD (Dia) [S11], BDD network (Network) [S11], CNF/BDD (CNF) [S26] , N-NCD (N-NCD, this work).

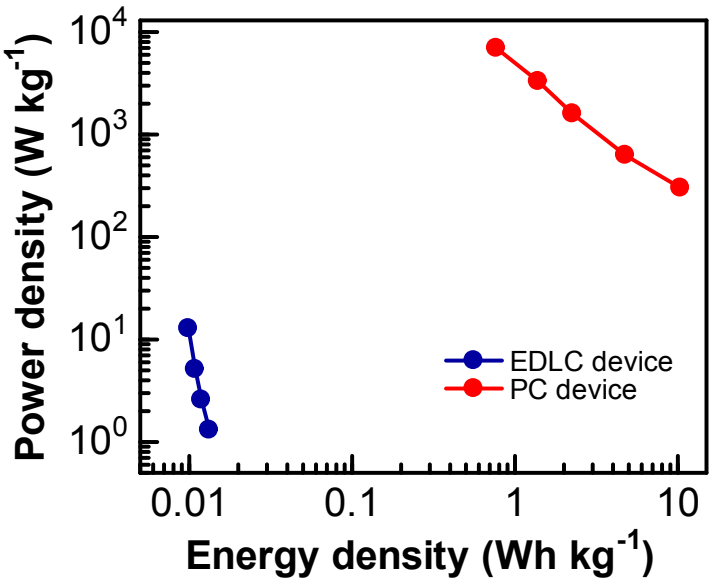

Figure S4. Ragone plots of diamond supercabatteries.

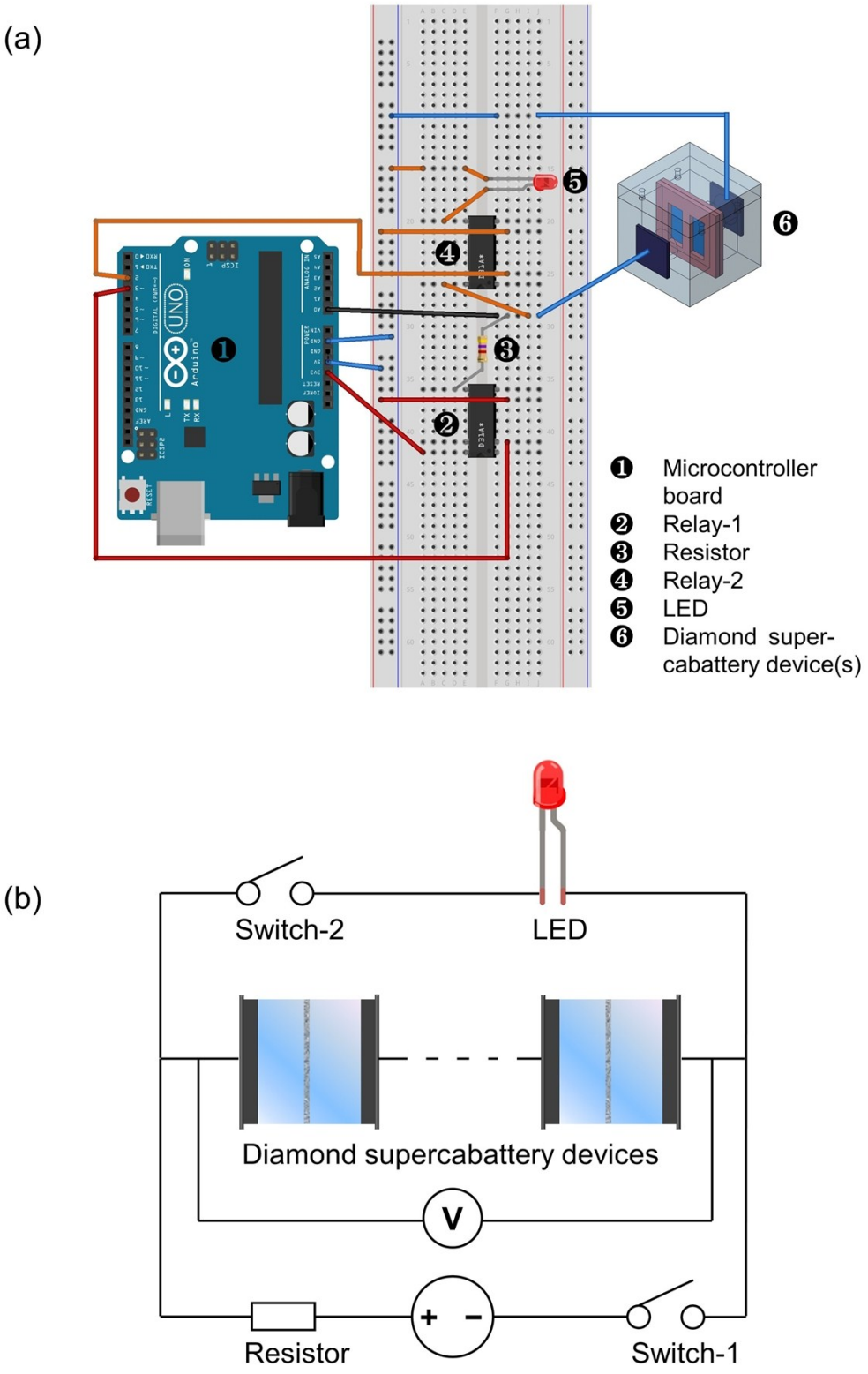

Figure S5. (a) The wiring diagram and (b) the electrical circuit diagram[S26] of one example stand-alone demonstrator to charge/discharge the diamond supercabattery device(s) and to light one LED. Reproduced with permission.[S26] Copyright, 2018 WILEY-VCH Verlag GmbH & Co. KGaA, Weinheim.

Supporting References

S1. B. Marcus, M. Mermoux, F. Vinet, A. Campargue, M. Chenevier, *Surf. Coat. Tech.* 1991, **47**, 608–617.

S2. Y. Shigesato, R. E. Boekenhauer, B. W. Sheldon, *Appl. Phys. Lett.* 1993, **63**, 314–316.

S3. G. Balestrino, M. Marinelli, E. Milani, A. Paoletti, P. Paroli, I. Pinter, A. Tebano, *Diamond Relat. Mater.* 1993, **2**, 389–392.

S4. P. W. May, Yu. A. Mankelevich, *J. Phys. Chem. C* 2008, **112**, 12432–12441.

S5. M. Sternbergt, P. Zapol, T. Frauenheimt, J. A. Carlisle, D. M. Gruen, L. A. Curtiss, *Mat. Res. Soc. Symp. Proc. MRS Proc.* 2001, **675**, W12.

S6. S. A. Kajihara, A. Antonelli, J. Bernhol, R. Car, *Phys. Rev. Lett.* 1991, **66**, 2010–2013.

S7. P. Zapol, M. Sternberg, L. A. Curtiss, T. Frauenheim, D. M. Gruen, *Phys. Rev. B* 2001, **65**, 045403.

S8. K. J. Sankaran, Y. F. Lin, W. B. Jian, H. C. Chen, K. Panda, B. Sundaravel, C. L. Dong, N. H. Tai, I N. Lin, *ACS Appl. Mater. Interfaces* 2013, **5**, 1294−1301.

S9. K. J. Sankaran, B. R. Huang, A. Saravanan, D. Manoharan, N. H. Tai, I. N. Lin, *Plasma Process. Polym.* 2016, **13**, 419–428.

S10. Y. Tzeng, S. Yeh, W. C. Yang, Y. Chu, *Sci. Rep.* 2014, **4**, 4531.

S11. S. Yu, N. Yang, H. Zhuang, S. Mandal, O. A. Williams, B. Yang, N. Huang and X. Jiang, *J. Mater. Chem. A*, 2017, **5**, 1778-1785.

S12. F. Gao, G. Lewes-Malandrakis, M. T. Wolfer, W. Müller-Sebert, P. Gentile, D. Aradilla, T. Schubert and C. E. Nebel, *Diamond Relat. Mater.*, 2015, **51**, 1-6.

S13. D. Aradilla, F. Gao, G. Lewes-Malandrakis, W. Müller-Sebert, D. Gaboriau, P. Gentile, B. Iliev, T. Schubert, S. Sadki, G. Bidan and C. E. Nebel, *Electrochem. Commun.*, 2016, **63**, 34-38.

S14. F. Gao, M. T. Wolfer and C. E. Nebel, *Carbon*, 2014, **80**, 833-840.

S15. K. Honda, T. N. Rao, D. A. Tryk, A. Fujishima, M. Watanabe, K. Yasui and H. Masuda, *J. Electrochem. Soc.*, 2000, **147**, 659-664.

S16. K. Honda, T. N. Rao, D. A. Tryk, A. Fujishima, M. Watanabe, K. Yasui and H. Masuda, *J. Electrochem. Soc.*, 2001, **148**, A668-A679.

S17. M. Yoshimura, K. Honda, R. Uchikado, T. Kondo, T. N. Rao, D. A. Tryk, A. Fujishima, Y. Sakamoto, K. Yasui and H. Masuda, *Diamond Relat. Mater.*, 2001, **10**, 620-626.

S18. C. Hébert, E. Scorsone, M. Mermoux and P. Bergonzo, *Carbon*, 2015, **90**, 102-109.

S19. T. Kondo, Y. Kodama, S. Ikezoe, K. Yajima, T. Aikawa and M. Yuasa, *Carbon*, 2014,

77, 783-789.

S20. V. Petrák, Z. Vlčková Živcová, H. Krýsová, O. Frank, A. Zukal, L. Klimša, J. Kopeček, A. Taylor, L. Kavan and V. Mortet, *Carbon*, 2017, **114**, 457-464.

S21. C. Hébert, J. P. Mazellier, E. Scorsone, M. Mermoux and P. Bergonzo, *Carbon*, 2014, **71**, 27-33.

S22. E. C. Almeida, A. F. Azevedo, M. R. Baldan, N. A. Braga, J. M. Rosolen and N. G. Ferreira, *Chem. Phys. Lett.*, 2007, **438**, 47-52.

S23. E. C. Almeida, M. R. Baldan, J. M. Rosolen and N. G. Ferreira, *Diamond Relat. Mater.*, 2008, **17**, 1529-1533.

S24. P. W. May, M. Clegg, T. A. Silva, H. Zanin, O. Fatibello-Filho, V. Celorrio, D. J. Fermin, C. C. Welch, G. Hazell, L. Fisher, A. Nobbs and B. Su, *J. Mater. Chem. B*, 2016, **4**, 5737-5746.

S25. W. Tong, K. Fox, A. Zamani, A. M. Turnley, K. Ganesan, A. Ahnood, R. Cicione, H. Meffin, S. Prawer, A. Stacey and D. J. Garrett, *Biomaterials*, 2016, **104**, 32-42.

S26. S. Yu, N. Yang, M. Vogel, S. Mandal, O. A. Williams, S. Jiang, H. Schönherr, B. Yang and X. Jiang, *Adv. Energy Mater.*, 2018, **8**, 1702947.

S27. M. Sawczak, M. Sobaszek, K. Siuzdak, J. Ryl, R. Bogdanowicz, K. Darowicki, M. Gazda and A. Cenian, *J. Electrochem. Soc.*, 2015, **162**, A2085-A2092.

S28. K. Siuzdak, R. Bogdanowicz, M. Sawczak and M. Sobaszek, *Nanoscale*, 2015, **7**, 551-558.

S29. M. Sobaszek, K. Siuzdak, M. Sawczak, J. Ryl and R. Bogdanowicz, *Thin Solid Films*, 2016, **601**, 35-40.

S30. C. Shi, H. Li, C. Li, M. Li, C. Qu and B. Yang, *Appl. Surf. Sci.*, 2015, **357, Part B**, 1380-1387.

S31. S. Yu, N. Yang, H. Zhuang, J. Meyer, S. Mandal, O. A. Williams, I. Lilge, H. Schönherr and X. Jiang, *J. Phys. Chem. C*, 2015, **119**, 18918-18926.

S32. F. Gao and C. E. Nebel, *Phys. Status Solidi A*, 2015, **212**, 2533-2538.

S33. C. Shi, C. Li, M. Li, H. Li, W. Dai, Y. Wu and B. Yang, *Appl. Surf. Sci.*, 2016, **360, Part A**, 315-322.